IEEE Access
Multidisciplinary | Rapid Review | Open Access Journal

Received August 2, 2020, accepted August 23, 2020, date of publication August 26, 2020, date of current version September 10, 2020.

Digital Object Identifier 10.1109/ACCESS.2020.3019692

Reliable Optical Performance Monitor: The Combination of Parallel Framework and Skip Connected Generative Adversarial Network

XIAOJIE FAN[1], FANG REN[1,2], JINGYU ZHANG[1], YIYING ZHANG[1], JINGJING NIU[1], AND JIANPING WANG[1]

[1]School of Computer and Communication Engineering, University of Science and Technology Beijing, Beijing 100083, China
[2]State Key Laboratory of Beijing Engineering and Technology Research Center for Convergence Networks and Ubiquitous Services, University of Science and Technology Beijing, Beijing 100083, China

Corresponding author: Fang Ren (renfang@ustb.edu.cn)

This work was supported in part by the Fundamental Research Funds for the Central Universities under Grant FRF-TP-19-016A2, and in part by the National Natural Science Foundation of China (NSFC) under Grant 61605004.

ABSTRACT Future optical network is developing towards highly heterogeneity and flexibility, which means that the various signals will be transmitted in the network and the optical performance monitor is more likely to encounter the signal beyond its monitoring range. When the signal beyond monitoring range (abnormal data) is input, the conventional optical performance monitoring (OPM) framework without the ability of data filtering will produce completely wrong results. Although the serial OPM framework has the ability of data filtering, it increases the processing time cost. We propose a novel parallel OPM framework, in which the judgement and analysis modules process the input data simultaneously to reduce the time cost. Moreover, the light-weight and high-performance skip connected generative adversarial network (GAN) trained only on the normal data (within the monitoring range) is proposed in the judgement module to filter the abnormal data in a fast-speed way (∼9 ms). In the simulation, eight common signals are used to test the performance of the skip connected GAN in the judgement module. The optimal area under the curve (AUC) value of 0.952 is obtained when the abnormal data is defined as 60 Gbps 64QAM signal. Besides, the impact of the latent vector length, the task weights, the weight of abnormal score, shifted K values and training data size on the model performance are studied.

INDEX TERMS Generative adversarial network (GAN), optical performance monitoring (OPM).

I. INTRODUCTION

With the expansion of the Internet users and the emergence of various services like cloud computing, artificial intelligence (AI) and internet of things (IoT), the optical network is becoming heterogeneous, dynamic and complex so as to ensure that massive data can be effectively transmitted [1]. Moreover, in order to maintain good operation and management of optical network, it is of great significance to use optical performance monitoring (OPM) along with bit-rate and modulation format identification (BR-MFI) in the network's intermediate nodes to accurately monitor the performance parameters of the transmitted signal (e.g. bit-rate, optical signal-to-noise ratio (OSNR), modulation format, etc.) [2]. These accurately monitored parameters, which are sent to the optical control layer, directly reflect the signal status and can provide as important decision basis for the management of optical network.

In the network's intermediate nodes, the traditional framework of the optical performance monitor consists of the data generation module and the data analysis module in sequence, which means that the monitor first collects signals to generate suitable data, and then analyzes the generated data to obtain the monitoring results. In order to obtain more accurate monitoring results, a large number of deep learning (DL) technologies such as deep neural networks (DNN) [3]–[7], the convolutional neural networks (CNN) [8]–[11], the long short-term memory (LSTM) [12], [13] and so on, which belong to the category of supervised learning are applied to the data analysis module for OPM and BR-FMI. Thanks to

The associate editor coordinating the review of this manuscript and approving it for publication was San-Liang Lee.

the capability of extracting and sharing the features, the DL technology is more powerful than machine learning (ML) technology.

The usage of these DL technologies which belong to the supervised learning class, can be separated into training stage and testing stage. It is noted that in the supervised learning, the training and testing sets are derived from the same monitoring range (the same data distribution). Otherwise, the DL model would produce completely wrong results. For instance, a DL model trained with multiple phase shift keying (MPSK) signals with the aim of identifying the signal type cannot get the correct results when the input data is quadrature amplitude modulation (QAM) signals. However, with the development of the optical network, the optical performance monitor would inevitably encounter the data which beyond its monitoring range (named as abnormal data). Worse still, the traditional monitoring framework does not have the ability of data filtering, and the input abnormal data would lead to the DL models in the data analysis module get wrong results.

In order to enhance the reliability of the optical performance monitor, a serial OPM framework and a generative adversarial network (GAN) with the encoder-decoder-encoder (EDE) structure were introduced with the purpose of filtering the abnormal data [14]. The judgement module is placed after the data generation module so as to filter the abnormal data before the data analysis module. The training set of the data analysis module is used to train the EDE based GAN in the judgement module to learn the distribution of the normal data which lie the monitoring range, which means that no additional data is required. The judgement module is loosely coupled with the data analysis module, which means that the DL models in the analysis module can continue to work without any modification. Compared with the idea of using the supervised learning method to identify the abundant abnormal data, our previous work [14] is low-cost and scalable, which greatly improve the reliability of monitoring. However, our previous work still has the following drawbacks: (1) The serial OPM framework increases the processing time of the input data. It is because the input data needs to be processed by each module successively. The more serial modules, the longer it takes. (2) The EDE based GAN model in the judgement module is complex and its performance is not good enough. Hence, a more advanced OPM framework as well as a more light-weight and high-performance algorithm in the judgement module are needed to obtain more reliable and fast optical performance monitoring.

In this article, we address the drawbacks in our previous work and propose a novel parallel OPM framework as well as the skip connected GAN model to realize reliable and fast optical performance monitoring. In the parallel OPM framework, the generated data is processed by the judgement module and the data analysis module in parallel, which shorten the processing time compared with the serial OPM framework. Moreover, the skip connected GAN is trained to learn the distribution of the input image data and the latent vector space. The skip connections in the generator of the GAN facilitate the multi-scale capture of the image space [15]. The discriminator not only helps the generator to learn the data distribution but also learns the distribution of the latent vectors by itself. In the data generation module, the data is generated by the asynchronous single channel sampling (ASCS) method. The performance of the skip connected GAN in the judgement module is verified by eight signals with diverse optical impairments (OSNR, differential group delay (DGD) and chromatic dispersion(CD)): 60/100 Gbps 4 quadrature amplitude modulation (QAM), 60/100 Gbps quadrature phase-shift keying (QPSK), 60/100 Gbps 64QAM, 60/100 Gbps 16QAM.

The remainder of this article is organized as follows. In Section II, the principles of the parallel OPM framework, asynchronous single channel sampling and the skip connected GAN model are illustrated and discussed. In Section III, the simulation set-up is presented and described. Moreover, the simulation results of the skip connected model is also presented and discussed. The conclusion of this article is summarized in Section IV.

II. METHODS

A. THE PARALLEL OPM FRAMEWORK

In order to maintain good control and management of the optical network, it is important to deploy optical performance monitors in the intermediate nodes. However, due to the expensive hardware cost and high sampling rate, the digital signal processing (DSP)-based coherent detection methods are not suitable to be deployed at the intermediate nodes [16]. Instead, with the advantage of cost-effective and low-speed sampling, the direct detection and asynchronous sampling (DDAS) method is used in this work. The performance parameters monitored by the optical performance monitors are sent to the control and management layer to formulate the management strategy for the network. However, there is a contradiction between the new signal generated with the upgrade of the optical network and the optical performance monitor with fixed monitoring range. Specifically, completely wrong monitoring results will be got when the new signal beyond the monitoring range of the optical performance monitor is input, which is a hidden danger for the management of the network. Therefore, to enhance the reliability of the monitor, a judgement module which can filter the abnormal data is needed.

The structure comparisons among the traditional OPM framework, the serial OPM framework and the new proposed parallel OPM framework are shown in Fig. 1. As far as we know, the parallel framework is first proposed in the OPM field by us. The data generation and analysis modules are the two modules existing in all three OPM frameworks. The judgement module only exists in the serial and parallel OPM frameworks. Therefore, the traditional OPM framework is unreliable. Moreover, the data processing time of each

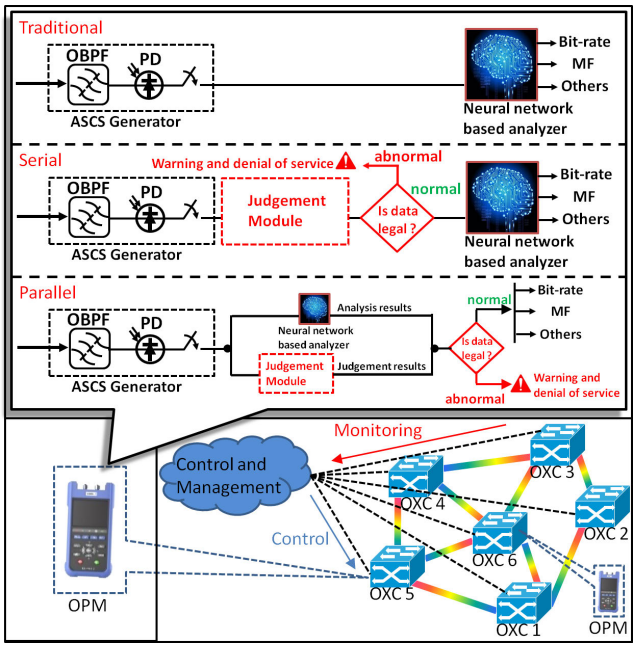

FIGURE 1. The structure comparisons among the traditional OPM framework, the serial OPM framework and the new proposed parallel OPM framework. OXC: optical cross-connect.

OPM framework is investigated to highlight the low time-cost advantage of the parallel OPM framework. The processing times of the traditional, serial and parallel OPM frameworks from the input data to the results are defined as t_{all}^{T}, t_{all}^{S} and t_{all}^{P}, respectively. The processing times of the generation, judgement and analysis modules are defined as t_G, t_J and t_A, respectively. In the traditional OPM framework, the input data will be processed by the data generation module and the data analysis module in sequence, which means that the processing time of the traditional OPM framework can be expressed as:

$$t_{all}^{T} = t_G + t_A \quad \textit{when} \text{ the input is normal/abnormal} \tag{1}$$

In the serial OPM framework, the input data will be processed by the data generation module and the judgement module. If the judgement module classifies the input data as normal data, then the input data needs to be processed by the data analysis module. Otherwise, the judgement module will produce a warning message and deny the service. The processing time of the serial OPM framework can be expressed as:

$$t_{all}^{S} = \begin{cases} t_G + t_J + t_A, & \text{when the input is normal} \\ t_G + t_J, & \textit{when} \text{ the input is abnormal} \end{cases} \tag{2}$$

In the parallel OPM framework, the input data will be processed by the data generation module firstly, and then processed by the judgement and analysis modules in parallel. If the judgement module classifies the input data as normal, the analysis results from the data analysis module is regarded as the monitoring results. Otherwise, the judgement module will produce the warning message and deny the service. The processing time of the parallel OPM framework can be expressed as:

$$t_{all}^{P} = \begin{cases} t_G + \max(t_J, t_A), & \text{when the input is normal} \\ t_G + t_J, & \textit{when} \text{ the input is abnormal} \end{cases} \tag{3}$$

Moreover, according to equations (1)-(3) and the size relationship between t_J and t_A, we can conclude as follows:

$$\begin{cases} \textit{if } t_J = t_A, \\ \quad \text{then} \begin{cases} t_{all}^{S} > t_{all}^{T} = t_{all}^{P}, & \text{when the input is normal} \\ t_{all}^{S} = t_{all}^{T} = t_{all}^{P}, & \text{when the input is abnormal} \end{cases} \\ \textit{if } t_J > t_A, \\ \quad \text{then} \begin{cases} t_{all}^{S} > t_{all}^{P} > t_{all}^{T}, & \text{when the input is normal} \\ t_{all}^{S} = t_{all}^{P} > t_{all}^{T}, & \text{when the input is abnormal} \end{cases} \\ \textit{if } t_J < t_A, \\ \quad \text{then} \begin{cases} t_{all}^{S} > t_{all}^{T} = t_{all}^{P}, & \text{when the input is normal} \\ t_{all}^{T} > t_{all}^{S} = t_{all}^{P}, & \text{when the input is abnormal} \end{cases} \end{cases} \tag{4}$$

According to our previous work [10], we take processing time of t_J = 9ms and t_A = 51ms from this work (shown in Section C, part III) and our previous OPM work [10] (which perform OPM based on ASCS images), respectively, as examples to analyze equation (4) concretely. According to equations (1)-(3), when the input is normal, the t_{all}^{T}, t_{all}^{S} and t_{all}^{P} equals to $(t_G + 51)$ ms, $(t_G + 60)$ms and $(t_G + 51)$ ms, respectively, and when the input is abnormal, the the t_{all}^{T}, t_{all}^{S} and t_{all}^{P} equals to $(t_G + 51)$ ms, $(t_G + 9)$ms and $(t_G + 9)$ ms, respectively. The result of the specific example is consistent with equation (4) when $t_J < t_A$. It is noted that in our parallel framework, the judgement module and analysis module are decoupled, which means the existing OPM works proposed by researchers can be applied in the analysis module without any modification. With the development of the research, the t_J and t_A are likely to be shorter and shorter. However, no matter what relationship between t_J and t_A is, equation (4) summarizes all the results. It is clear that the t_{all}^{P} is definitely not larger than the t_{all}^{S}, which demonstrates the superiority of the parallel OPM framework. Moreover, the parallel structure requires higher demand for the computing power of the optical performance monitor, but with the development of hardware equipments, the computing power is no longer an obstacle.

B. ASYNCHRONOUS SINGLE CHANNEL SAMPLING

As a typical representative of the DDAS method, the ASCS method is used in the data generation module to generate the phase portrait images (".png" format), which are the data format that the subsequent modules will need to process. Due to the fact that no clock information is needed, the ASCS method with the single-tap sampling way is economical and uncomplicated [17], [18]. Fig. 2 shows the principle of the ASCS method for generating the phase portrait image.

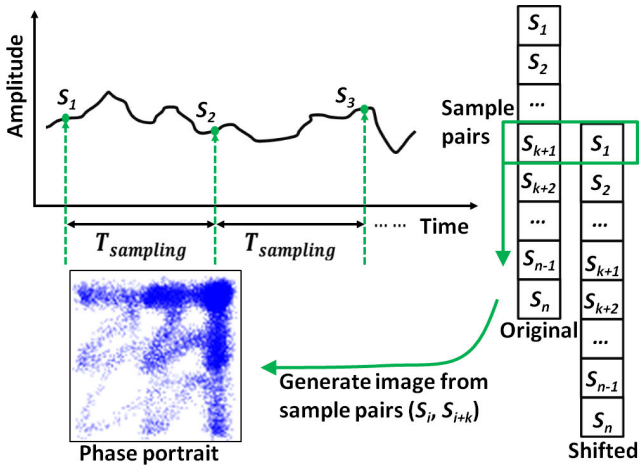

FIGURE 2. The principle of the ASCS method for generating the phase portrait image.

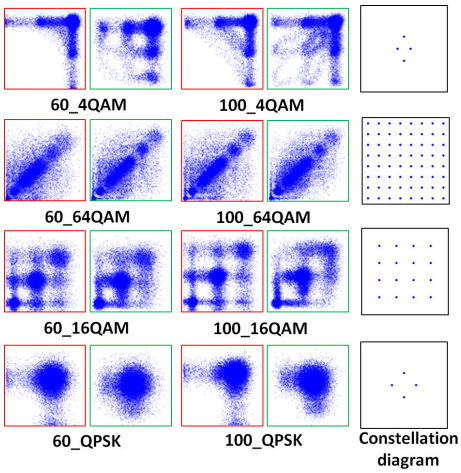

FIGURE 3. The typical phase portrait images of the eight signals influenced by impairments. For each signal type, the image with red border is generated when CD = 0 ps/nm, DGD = 0 ps and OSNR = 16 dB. the image with green border is generated when CD = 150 ps/nm, DGD = 3 ps and OSNR = 18 dB. The respective constellation diagrams of different modulation types is shown at the end of each row.

Firstly, the photodetector (PD) is used to directly convert the optical signal into the electrical signal. The intensity of the optical signal will be converted into the voltage amplitude of the electric signal. Then, the original sample sequence $S_1, S_2 \cdots S_N$ is acquired by single-tap sampling the electric signal at the frequency of $1/T_{\text{sampling}}$. By shifting k samples of the original sample sequence, the shifted sample sequence is obtained. The sample pairs of (S_i, S_{i+k}) are collected from the original and shifted sample sequences. Finally, 20000 collected sample pairs are used to plot a phase portrait image. Some typical phase portrait images ($k = 10$) of the eight different signals and their respective constellation diagrams are shown in Fig. 3. It is noted that we use geometric shaping (GS) [19] technology to redesign the regular 4QAM constellation into diamond shape constellation to make distinction with QPSK constellation diagram. It is clear that the phase portrait image can reflect the influence of bit-rate, signal format and signal impairments in visual information, which is the basis condition for the judgement and analysis modules to work properly. It is noted that this work is finished mainly from the perspective of image processing, so the phase portrait images with specific format ('.png') are transformed from raw data. However, this transformation may lead to the loss of information and further influence the model performance, which remains to be studied in the future.

C. THE SKIP CONNECTED GAN IN JUDGEMENT MODULE

For the purpose of filtering the abnormal data, the unsupervised GAN is used to design the DL model. The GAN proposed by Goodfellow *et al.* [20] is a hot spot in the research of DL [21]–[26]. The principle of the GAN is founded on the rivalry of two networks within a zero-sum game framework. The first network named as generator (G) is used to capture the input data's distribution, whilst, the second network named as discriminator (D) is used to predict the correct class (i.e., normal or abnormal). Each network is constantly improving its ability in the competition until they reach a balance. With the help of GAN, the designed DL model has a stronger ability to learn the normal data distribution so as to filter the abnormal data. Moreover, in the EDE based GAN model which we proposed before, the generator is the structure of the encoder-decoder-encoder for the purpose of learning the distribution of the image and latent spaces simultaneously. This kind of generator is complex and its performance needs to be improved. Here, we simplify the encoder-decoder-encoder structure of the generator to the encoder-decoder structure, and skip connections are added to enable the multi-scale capture of the image space. The encoder-decoder structure with skip connections is similar to the UNet style which is good at capturing the image details [15]. Different from the EDE based GAN which learns the distribution of image and latent spaces simultaneously in the generator, the skip connected GAN learns the distribution of image and latent spaces in the generator and discriminator, respectively. With the simplified structure of the generator and the added skip connections, the new proposed skip connected GAN model is light-weight and high-performance.

The structure of the skip connected GAN is illustrated in Fig. 4, which consists of the generator (G) and the discriminator (D) networks. In the network G, the input image I with the shape of $32 \times 32 \times 3$ is down-sampled by the encoder sub-network G_E to the low-dimensional feature with the shape of $1 \times 1 \times 512$, then, the low-dimensional feature is up-sampled to reconstruct the input image I as $\hat{I}$ by the decoder sub-network G_D. The sub-network G_E has four layers, each of which consists of the Convolutional operation, LeakeyReLu and BatchNorm. As the symmetrical structure of G_E, the G_D also has four layers, each of which consists of the Convolutional transpose operation, BatchNorm and

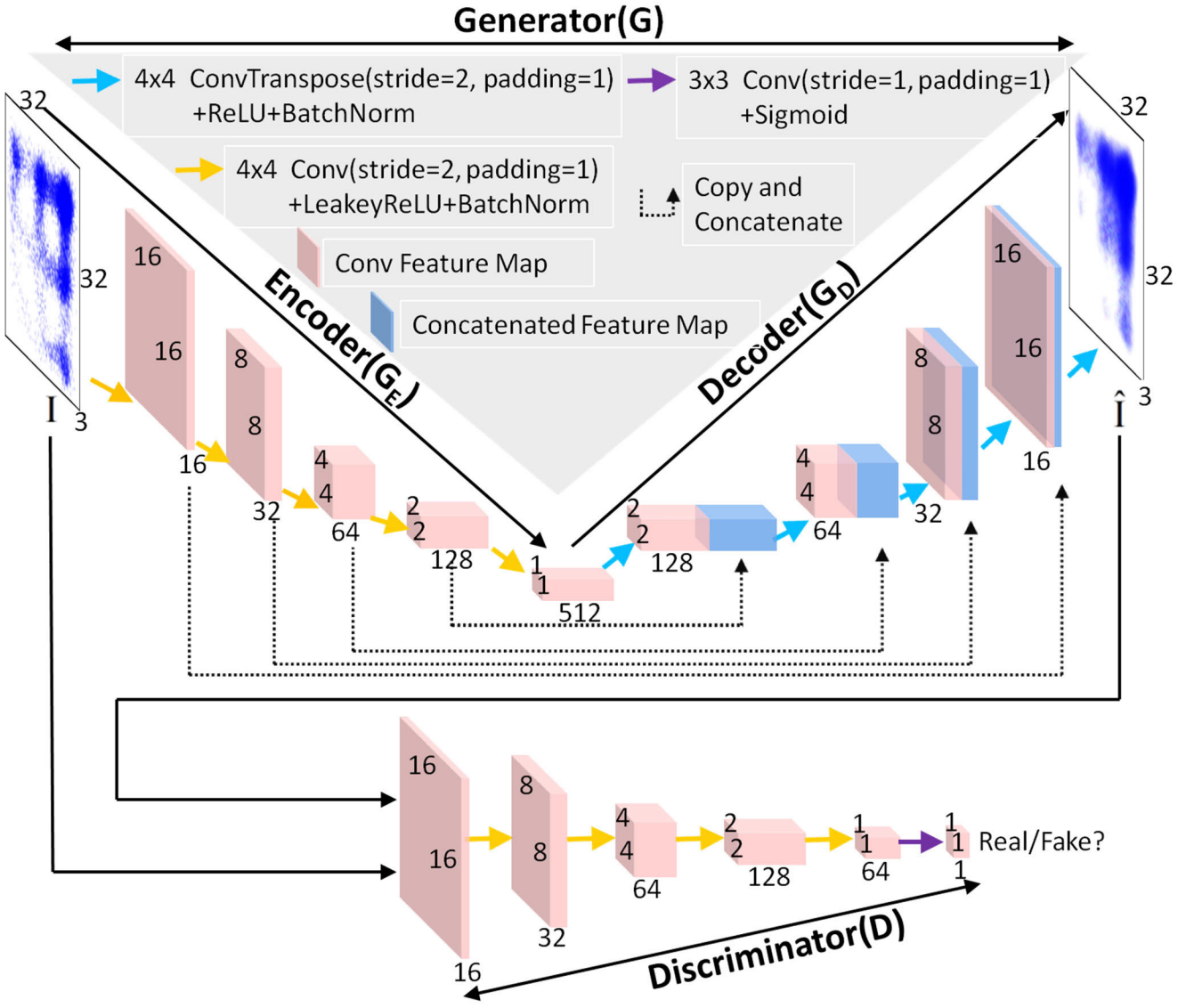

FIGURE 4. The detailed structure of the skip connected GAN in the judgement module.

ReLu. Moreover, the G_D uses the method of the skip connection so that every down-sampling layer in the G_E is copied and concatenated to its homologous up-sampling layer in the G_D. The benefit of using the skip connections is that they provide direct feature transfer between the layers so that both the local and global information is probed and better image reconstruction is obtained. The network D is used to classify the real image I from the fake image $\hat{I}$ generated by G during training. Besides, the network D also extracts the latent feature vector of the input image and the reconstructed image from the Penultimate layer with shape of $1 \times 1 \times 64$. Other detail configurations such as the stride, padding, filter size and so on are clearly illustrated in Fig. 4. The whole skip connected GAN is trained on the normal data, and tested on both the abnormal and normal data. In the training phase, the skip connected GAN learns the distribution of the normal data in the image and latent vector spaces. In the testing phase, since the model is never trained on the abnormal data, the reconstruction loss of the abnormal data is higher than the reconstruction loss of the normal data, which can be used as the standard to discriminate the normal from abnormal data. In order to train and test the skip connected GAN, a dataset $\{I_i\}^{m+n}$ is split into the training set $\{I_i\}^m$ and testing set $\{I_i\}^n$, where $I_i \in R^{32\times32\times3}$ is the input image, $m+n$ is the total number of images. Moreover, the training set $\{I_i\}^m$ only contains m normal images and the corresponding label $y_i = 0$ denotes normal data. The testing set $\{I_i\}^n$ contains n normal and abnormal images and the corresponding label $y_i \in \{0, 1\}$ denotes normal and abnormal data, respectively.

During the training phase, the adversarial loss, the reconstruction loss and the latent vector loss are combined to train the model. The adversarial loss is used to impose G to reconstruct image authentically, and D to classify the real image from the generated image. The adversarial loss is denoted as:

$$loss_{adv} = E_{x\sim p_x}\left[\log D\left(I_i\right)\right] + E_{x\sim p_x}\left[\log\left(1 - D\left(\hat{I}_i\right)\right)\right] \tag{5}$$

The reconstruction loss is used to capture the distribution of the input normal data and reconstruct the input image as similarly as possible. The reconstruction loss defined by the L_1 distance is expressed as:

$$loss_{rec} = E_{x\sim p_x}\left|I_i - \hat{I}_i\right|_1 \tag{6}$$

The latent vector loss is used to reconstruct the latent vector from the input and the generated images as akin as possible. The Penultimate layer of the D is used as the extracted latent vector of the input image and the generated image. The latent vector loss is expressed as:

$$loss_{lat} = E_{x\sim p_x}\left|f\left(I_i\right) - f\left(\hat{I}_i\right)\right|_2 \tag{7}$$

where the $f(\cdot)$ is the output of the $D's$ penultimate layer. Finally, the combined total training loss can be defined as the weighted sum of the three individual losses above:

$$loss_{total} = loss_{rec} + \lambda_1 loss_{adv} + \lambda_2 loss_{lat} \tag{8}$$

where the weight parameters λ_1 and λ_2 are used to adjust the influence of $loss_{adv}$ and $loss_{lat}$, respectively.

During the testing phase, the abnormal score is defined to measure how likely a test image is to be an abnormal data. The input test image will be regarded as abnormal data when its abnormal score is higher than a certain threshold. The abnormal score $S\left(I'\right)$ of the given test image I' can be expressed as:

$$S\left(I'\right) = \lambda_3 R\left(I'\right) + (1 - \lambda_3) L\left(I'\right) \tag{9}$$

where $R\left(I'\right)$ is the reconstruction loss between the generated and input images as stated in equation (6). $L\left(I'\right)$ is the latent vector loss between the extracted feature vectors of the input and generated images as stated in equation (7). λ_3 is the weight parameter of the abnormal score balancing the influence of the $R\left(I'\right)$ and $L\left(I'\right)$. The entire testing set's abnormal scores are standardized to the range of 0 and 1.

III. SYSTEM SETUP AND RESULTS

The VPItransmissionMaker and the Pytorch library are used to set up the simulation system as illustrated in Fig. 5. Eight signals (60/100 Gbps 64QAM, 60/100 Gbps 16QAM, 60/100 Gbps QPSK, 60/100 Gbps 4QAM) are prepared in the transmitter to be transmitted over a single-mode fiber (SMF). During the transmission, the variable optical attenuator (VOA), the erbium-doped fiber amplifier (EDFA) and the CD/PMD emulator are applied to add OSNR and

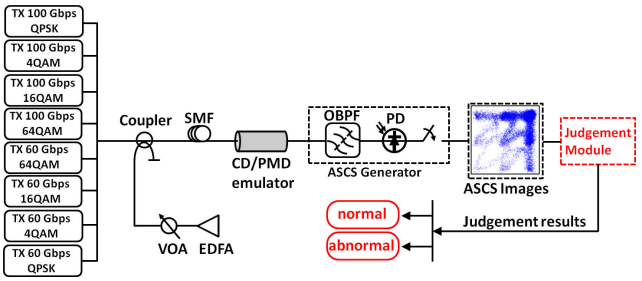

FIGURE 5. The simulation platform is established to generate signal data and check the judgement module's performance.

CD/DGD, respectively. The OSNR is adjusted at intervals of 2 dB between 10 dB and 28 dB. The CD is adjusted at intervals of 50 ps/nm between 0 ps/nm and 450 ps/nm. The DGD is adjusted at intervals of 1 ps between 0 ps and 10 ps. Then, the ASCS method (sampling rate: 1 GHz) in the generation module is applied to generate the ASCS images (".png" format). Finally, the generated image is used to check the judgement module's performance.

For each signal type, due to the combinations of the OSNR, CD and DGD values, 1100 ($10 \times 10 \times 11$) images are collected. Thus, a big dataset which contains 8800 (8×1100) images is established for the eight signals ($k = 10$). In order to conduct a comprehensive simulation of different monitoring ranges, we select each signal type as the abnormal (1100 images) while the rest as the normal (7700 images) to obtain eight different monitoring ranges. Moreover, for each monitoring range, we randomly pick 1100 images from the normal data and merge them with the abnormal data as the testing set (2200 images), and the remaining 6600 images become the training set. It is noted that the training set size of 6600 is selected according to the time cost of training, readers can adjust the size of training set according to your own situation. Totally, eight pairs of training sets and testing sets with different monitoring ranges are prepared to train and verify the performance of the skip connected GAN in the judgement module.

Two models in the judgement module are used for the performance comparison. when $\lambda_1 = 2$, $\lambda_2 = 3$ and $\lambda_3 = 0.4$, the first skip connected GAN model named as "GAN 1" is trained, and the second model named as "GAN 2" without the skip connections is also trained. The weight parameter's influence of the different losses and the abnormal scores are discussed in the section 3.2 and 3.3, respectively. These models are optimized via Adam [27] optimizer with the momentums $\beta_1 = 0.52$, $\beta_2 = 0.999$ and learning rate $lr = 2e^{-3}$. Moreover, the area under the curve (AUC) of the receiver operating characteristics (ROC) is used to evaluate the model performance. The ROC is a curve plotted by the true positive rates (TPR) and false positive rates (FPR) with varying threshold values, and the AUC is defined as the area bounded by the coordinate axis under the ROC curve. Each point on the ROC curve corresponds to a specific threshold, and a threshold determine the classification accuracy. The

AUC represents the probability that the positive sample ranks ahead of the negative sample, which is independent with the threshold. However, the classification accuracy is related to the threshold. The AUC value (the higher the better) is usually used to evaluate the performance of binary classifiers, so it is suitable to use the AUC value to evaluate our model which predicts two classes: normal or abnormal.

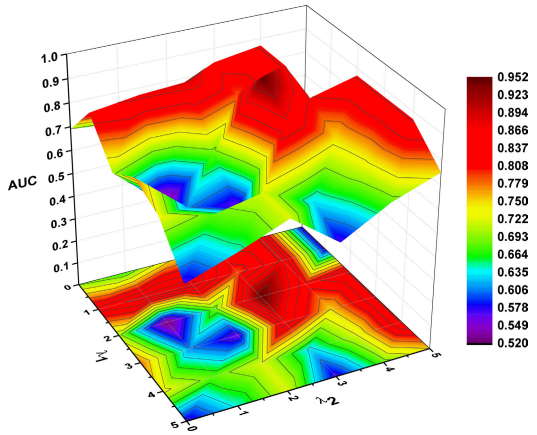

FIGURE 6. The model performance influenced by the task weights.

A. IMPACT OF THE TASK WEIGHTS, LATENT VECTOR LENGTH AND SHIFTED K VALUE

The impact of the task weights λ_1 and λ_2 on the "GAN 1" (abnormal type: 60 Gbps 64QAM, $\lambda_3 = 0.4$, latent vector length equals 64 and $k = 10$) is considered. The results are shown in Fig. 6. The value range of λ_1 and λ_2 are both from 0 to 5 with step 1. Obviously, the model performance dose not change regularly. Only by lots of simulation experiments, the impact of the task weights can be analyzed. The performance is relatively poor in the areas when $\lambda_1 > 4$ or $\lambda_2 < 2$. It is significant that when $\lambda_1 = 2$ and $\lambda_2 = 3$, the model obtain the highest performance (AUC = 0.952).

Besides, when the $\lambda_1 = 2$, $\lambda_2 = 3, \lambda_3 = 0.4$ and $k = 10$, the AUC values influenced by the latent vector length of the "GAN 1" under different monitoring range are shown in Fig. 7. The latent vector is in the Penultimate layer of the discriminator network, and the length of the latent vector means the number of the feature map channels. The latent vector lengths of 32, 64, 100, 256 and 512 are used to verify the model performance. It can be seen that when the latent vector length equals 64, the optimal model performance is obtained. However, as long as the length is more than or less than 64, the model performance would deteriorate. It is because that the latent vector length directly affects the model's ability to probe the distribution of the data in the latent space. Specifically, too short length would make the model unable to probe the complete data distribution. Too long length would lead to redundant information.

Moreover, the AUC performance of "GAN 1" under different monitoring range influence by the shifted k values when $\lambda_1 = 2$, $\lambda_2 = 3$, $\lambda_3 = 0.4$, latent vector length equals

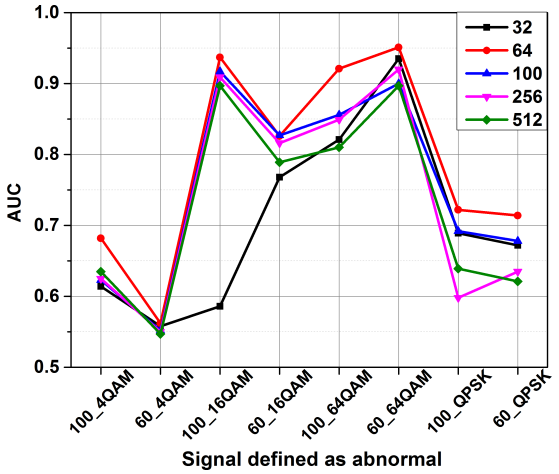

FIGURE 7. The model performance influenced by the latent vector length when different signal are defined as abnormal.

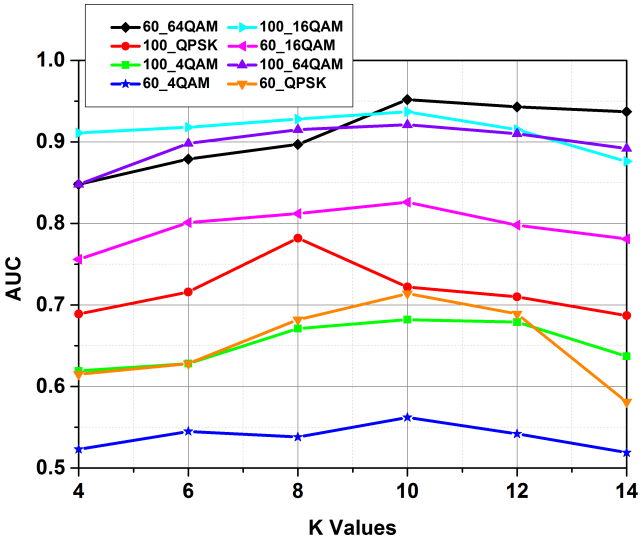

FIGURE 8. The model performance influenced by the shifted K values.

64 is shown in Fig. 8. The value range of k is from 4 to 14 with step 2. For k values of 4, 6, 8, 12 and 14, we use the ASCS method to generate the training and testing sets the same way as $k = 10$ for different monitoring ranges. It is clear from Fig. 8 that when $k = 10$ most monitoring ranges obtain the optimal AUC performance, except when 100 Gbps QPSK is defined as abnormal whose optimal AUC is obtained when $k = 6$. Moreover, some typical phase portrait images of eight signal types under different K values are shown in Fig. 9. For MQAM signals, it is clear that a K value smaller than 10 closes the phase portraits along the diagonal or edges, while a K value bigger than 10 increases the expansibility of the sample points, which lead to the underestimation of performance. For QPSK signals, when K value is bigger than 8 or 10, the sample points shrink inward. Therefore, when K equals 10, the phase portraits of most signal types can show sufficient information for model to learn.

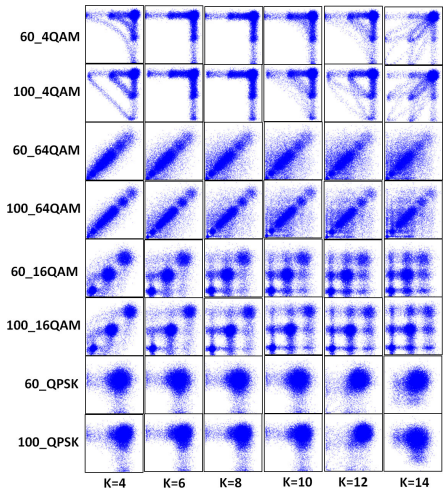

FIGURE 9. The typical phase portrait images (CD = 0 ps/nm, DGD = 0 ps and OSNR = 16 dB) of eight signal types under different K values.

The task weights, latent vector length and shifted k values have a direct impact on the model performance, so it is essential to pick the apt parameter values. Under the simulation conditions in this article, the best model performance is obtained when $\lambda_1 = 2$, $\lambda_2 = 3$, latent vector length equals 64 and $k = 10$.

B. WEIGHT OF ABNORMAL SCORE AND FEATURE VISUALIZATION

When the 60 Gbps 64QAM is defined as the abnormal signal, we take the "GAN 1" ($\lambda_1 = 2, \lambda_2 = 3$, latent vector length equals 64 and $k = 10$) as the research object. During the testing phase, the histogram of the abnormal scores affected by the abnormal score weight λ_3 is illustrated in Fig. 10. According to equation (9), the weight λ_3 is used to balance the influence of the $R(I')$ and $L(I')$. The λ_3 ranges from 0 to 1. The smaller the value of λ_3 is, the greater the effect of $L(I')$ on the abnormal score is. On the contrary, the larger the value of λ_3 is, the greater the effect of $R(I')$ on the abnormal score is. A typical histogram is plotted when λ_3 equals 0, 0.2, 0.4, 0.6, 0.8 and 1, respectively. It is clear that when λ_3 equals 0.4, the abnormal score's distribution of the normal images and the abnormal images are highly differentiated, and the optimal AUC (0.952) is obtained. Furthermore, the t-SNE [28] plot of the latent vector produced by the discriminator's Penultimate layer is shown in Fig. 11. The original high-dimension latent vectors are reduced to low-dimension vectors for the purpose of visualization. As shown in Fig. 11, there is a obvious boundary between the abnormal and normal data, which means that the discriminator has been able to discriminate the normal data from the abnormal data.

C. PERFORMANCE OF THE JUDGEMENT MODULE

Based on the determined optimal parameters, the AUC values of the "GAN 1", "GAN 2" and previously proposed "EDE GAN" when different signals are defined as the abnormal ones is shown in Fig. 12. No matter which signal is defined as abnormal, the "GAN 2" has the lowest AUC among the three models. The AUC values of the "GAN 1" is higher than the AUC values of the "EDE GAN" in almost all cases, except

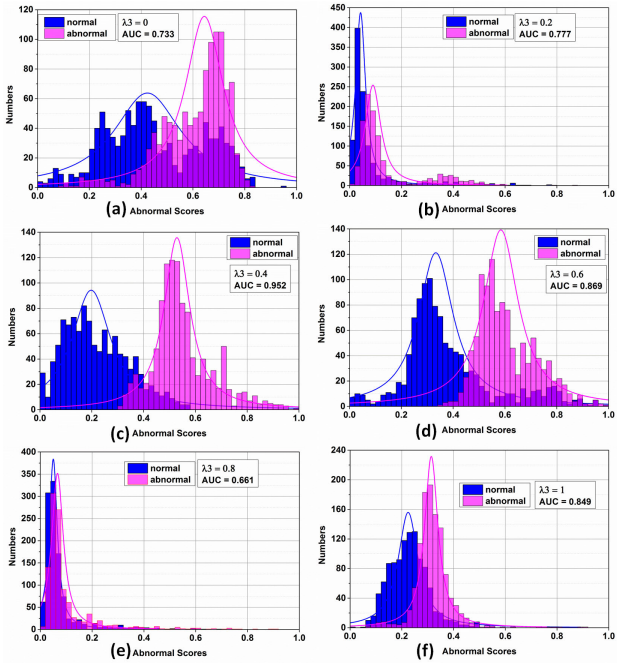

FIGURE 10. The histogram of the abnormal scores influenced by the λ_3 for the testing set. The Lorentz distribution curves of the histogram are plotted.

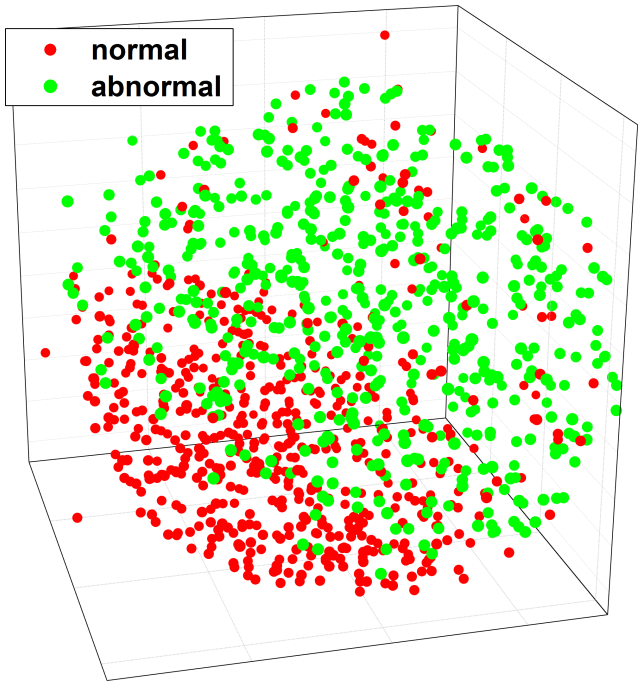

FIGURE 11. The t-SNE plot of the latent vector produced by the discriminator's penultimate layer.

TABLE 1. Number of parameters and consuming time for "GAN 1" and "EDE GAN".

	Number of Parameters	Total Time	Mean Time
GAN 1	2924340	20.1164 s	9.1438 ms
EDE GAN	3208203	26.2387 s	11.9267 ms

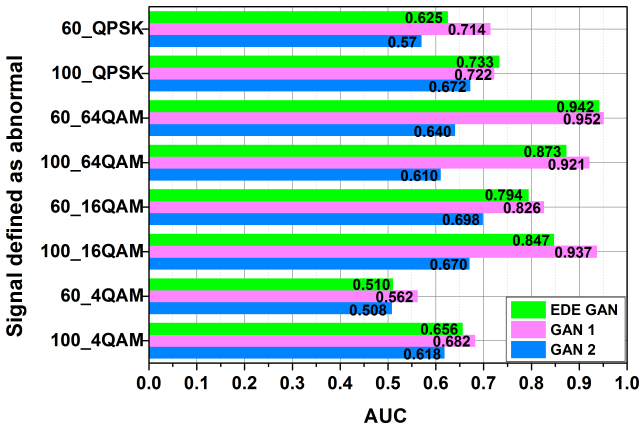

FIGURE 12. The AUC values of the "GAN 1", "GAN 2" and previously proposed "EDE GAN" when different signal defined as the abnormal.

the case that 100 Gbps QPSK is defined as the abnormal. The highest AUC value 0.952 of the "GAN 1" is obtained when the abnormal signal is defined as 60 Gbps 64QAM. Moreover, in order to compare the cost performance between the "GAN 1" and "EDE GAN", the number of parameters, the total and mean processing times are recorded in Table 1. Based on an Intel Core i7-6700 CPU, we record the total and mean times by using the "GAN 1" and "EDE GAN" models to process the images in testing set (2200 images, abnormal type: 60 Gbps 64QAM) one by one. It is found that with less number of parameters, the "GAN 1" model takes about 9 ms to process a single image, which is faster than the processing time of the "EDE GAN" model (∼12 ms). Too many parameters will slow down the processing speed. Thanks to the simplified structure, the "GAN 1" is light-weighted and fast. The above results show that the simplified model structure and the added skip connections not only shorten the processing time but also improve the model performance.

Chose the "GAN 1" and "GAN 2" as the research object (abnormal signal: 60 Gbps 64QAM), the typical input and reconstructed images are depicted in Fig. 13. The abnormal images have red border. The input images are revealed in Fig. 13(a). The reconstructed images by the "GAN 1" are shown in Fig. 13(b), and the reconstructed images by the "GAN 2" are shown in Fig. 13(c). Moreover, the numbers displayed on the top of the reconstructed images are the correlation between the reconstructed and the input images. The "GAN 1" is capable of reconstructing both normal and abnormal images and achieves better reconstruction performance than the "GAN 2", which means that the skip

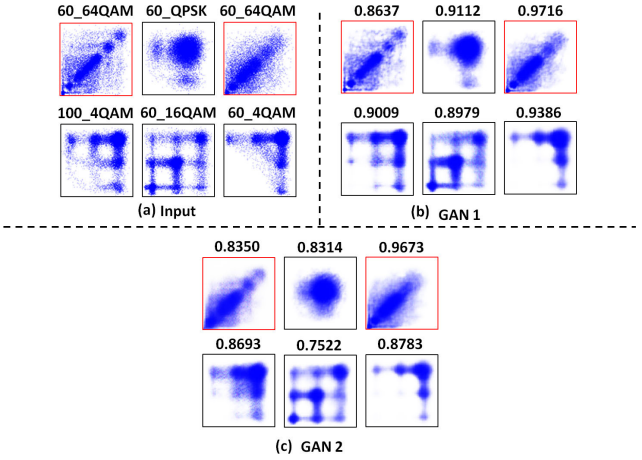

FIGURE 13. (a) The typical images in the testing set. (b) The reconstructed images by the "GAN 1". (c). The reconstructed images by the "GAN 2". The red border of the image represents the abnormal data. The numbers displayed on the top of the reconstructed images are the correlation between the reconstructed and the input images.

connections is powerful and it can capture the distribution of both domains in the image space. Since the "GAN 1" cannot make a clear distinction between normal and abnormal data in the image space, the obvious distinction is reflected in the latent vector space, which is discussed in the above section B.

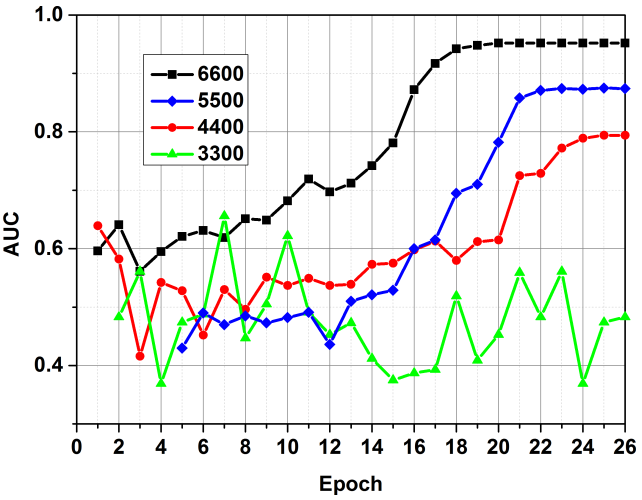

FIGURE 14. The AUC performance at different epochs for different sizes of training set.

Then, in order to explore the limit of the "GAN 1" performance, we continue to reduce the training data size from original 6600 to 5500, 4400 and 3300, and measure the AUC values using the testing set at different epochs, as shown in Fig. 14. When the training data size is 6600, the AUC curve converges at epoch 19. When the training data size is 5500, the AUC curve converges at epoch 22. When the training data size is 4400, the AUC curve converges at epoch 24. Nevertheless, when the training data size continue to reduce to 3300, the AUC curve cannot converge anymore.

We can conclude that with the reduction of the training data size, the AUC curve is more unstable and takes more epochs to get convergence, and finally, the AUC curve fails to get convergence when the training data size is 3300, since it is difficult for "GAN 1" model to learn the data distribution from the insufficient data size.

IV. CONCLUSION

A novel parallel OPM framework with skip connected GAN is proposed to filter abnormal signals, which improves the reliability of the optical performance monitor. The judgement and analysis modules are parallel organized in the OPM framework to process the input data simultaneously, which is faster than the serial OPM framework. Moreover, the proposed skip connected GAN simplifies the EDE based GAN by means of an encoder-decoder structure together with skip connections, which is light-weight and high-performance. When the 60 Gbps 64QAM signal is defined as the abnormal one, the skip connected GAN obtains the optimal AUC performance (0.952). When a single image is input, the average processing time of the skip connected GAN is around 9 ms. The impact of the latent vector length, the task weights, the weight of abnormal score, shifted K values and training data size on the performance of the model are studied. The parallel OPM framework and the skip connected GAN further improve the reliability and reduce the processing time, which is meaningful to the upgrading of the network.

REFERENCES

[1] Q. Zhuge and W. Hu, "Application of machine learning in elastic optical networks," in *Proc. Eur. Conf. Opt. Commun. (ECOC)*, Rome, Italy, Sep. 2018, pp. 1–3.
[2] Z. Dong, F. N. Khan, Q. Sui, K. Zhong, C. Lu, and A. P. T. Lau, "Optical performance monitoring: A review of current and future technologies," *J. Lightw. Technol.*, vol. 34, no. 2, pp. 525–543, Jan. 15, 2016.
[3] F. N. Khan, K. Zhong, X. Zhou, W. H. Al-Arashi, C. Yu, C. Lu, and A. P. T. Lau, "Joint OSNR monitoring and modulation format identification in digital coherent receivers using deep neural networks," *Opt. Express*, vol. 25, no. 15, pp. 17767–17776, Jul. 2017.
[4] F. N. Khan, T. S. R. Shen, Y. Zhou, A. P. T. Lau, and C. Lu, "Optical performance monitoring using artificial neural networks trained with empirical moments of asynchronously sampled signal amplitudes," *IEEE Photon. Technol. Lett.*, vol. 24, no. 12, pp. 982–984, Jun. 15, 2012.
[5] F. N. Khan, Y. Zhou, Q. Sui, and A. P. T. Lau, "Non-data-aided joint bit-rate and modulation format identification for next-generation heterogeneous optical networks," *Opt. Fiber Technol.*, vol. 20, no. 2, pp. 68–74, Mar. 2014.
[6] Z. Wan, Z. Yu, L. Shu, Y. Zhao, H. Zhang, and K. Xu, "Intelligent optical performance monitor using multi-task learning based artificial neural network," *Opt. Express*, vol. 27, no. 8, pp. 11281–11291, 2019.
[7] Y. Cheng, S. Fu, M. Tang, and D. Liu, "Multi-task deep neural network (MT-DNN) enabled optical performance monitoring from directly detected PDM-QAM signals," *Opt. Express*, vol. 27, no. 13, pp. 19062–19074, Jun. 2019.
[8] D. Wang, M. Zhang, J. Li, Z. Li, J. Li, C. Song, and X. Chen, "Intelligent constellation diagram analyzer using convolutional neural network-based deep learning," *Opt. Express*, vol. 25, no. 15, pp. 17150–17166, 2017.
[9] D. Wang, M. Zhang, Z. Li, J. Li, M. Fu, Y. Cui, and X. Chen, "Modulation format recognition and OSNR estimation using CNN-based deep learning," *IEEE Photon. Technol. Lett.*, vol. 29, no. 19, pp. 1667–1670, Oct. 1, 2017.
[10] X. Fan, L. Wang, F. Ren, Y. Xie, X. Lu, Y. Zhang, T. Zhangsun, W. Chen, and J. Wang, "Feature fusion-based multi-task ConvNet for simultaneous optical performance monitoring and bit-rate/modulation format identification," *IEEE Access*, vol. 7, pp. 126709–126719, 2019.
[11] X. Fan, Y. Xie, F. Ren, Y. Zhang, X. Huang, W. Chen, T. Zhangsun, and J. Wang, "Joint optical performance monitoring and modulation format/bit-rate identification by CNN-based multi-task learning," *IEEE Photon. J.*, vol. 10, no. 5, Oct. 2018, Art. no. 7906712.
[12] Z. Wang, A. Yang, P. Guo, and P. He, "OSNR and nonlinear noise power estimation for optical fiber communication systems using LSTM based deep learning technique," *Opt. Express*, vol. 26, no. 16, p. 21346, 2018.
[13] C. Wang, S. Fu, Z. Xiao, M. Tang, and D. Liu, "Long short-term memory neural network (LSTM-NN) enabled accurate optical signal-to-noise ratio (OSNR) monitoring," *J. Lightw. Technol.*, vol. 37, no. 16, pp. 4140–4146, Aug. 15, 2019.
[14] X. Fan, Y. Su, T. Dong, Y. Jie, Y. Zhang, F. Ren, J. Niu, J. Zhang, and J. Wang, "Enhancing the credibility of the optical performance monitor with adversarial training," *IEEE Access*, vol. 8, pp. 75682–75690, 2020.
[15] O. Ronneberger, P. Fischer, and T. Brox, "U-Net: Convolutional networks for biomedical image segmentation," in *Proc. Int. Conf. Med. Image Comput. Comput.-Assist. Intervent.*, 2015, pp. 234–241.
[16] D. Wang, M. Wang, M. Zhang, Z. Zhang, H. Yang, J. Li, J. Li, and X. Chen, "Cost-effective and data size-adaptive OPM at intermediated node using convolutional neural network-based image processor," *Opt. Express*, vol. 27, no. 7, pp. 9403–9419, 2019.
[17] Y. Yu and C. Yu, "OSNR monitoring by using single sampling channel generated 2-D phase portrait," in *Proc. Opt. Fiber Commun. Conf.*, 2014, pp. 1–3.
[18] Y. Yu and C. Yu, "Optical signal to noise ratio monitoring using variable phase difference phase portrait with software synchronization," *Opt. Express*, vol. 23, no. 9, pp. 11284–11289, 2015.
[19] Z. Qu and I. B. Djordjevic, "On the probabilistic shaping and geometric shaping in optical communication systems," *IEEE Access*, vol. 7, pp. 21454–21464, 2019.
[20] I. Goodfellow, J. Pouget-Abadie, M. Mirza, B. Xu, D. Warde-Farley, S. Ozair, A. Courville, and Y. Bengio, "Generative adversarial nets," in *Proc. Adv. Neural Inf. Process. Syst.*, pp. 2672–2680, 2014.
[21] A. Radford, L. Metz, and S. Chintala, "Unsupervised representation learning with deep convolutional generative adversarial networks," *Comput. Sci.*, vol. 2, no. 3, pp. 34–38, Nov. 2015.
[22] Y. Zhao, S. Takaki, H.-T. Luong, J. Yamagishi, D. Saito, and N. Minematsu, "Wasserstein GAN and waveform loss-based acoustic model training for multi-speaker text-to-speech synthesis systems using a WaveNet vocoder," *IEEE Access*, vol. 6, pp. 60478–60488, 2018.
[23] Y. Saito, S. Takamichi, and H. Saruwatari, "Statistical parametric speech synthesis incorporating generative adversarial networks," *IEEE/ACM Trans. Audio, Speech, Lang. Process.*, vol. 26, no. 1, pp. 84–96, Jan. 2018.
[24] P. Isola, J.-Y. Zhu, T. Zhou, and A. A. Efros, "Image-to-image translation with conditional adversarial networks," in *Proc. IEEE Conf. Comput. Vis. Pattern Recognit. (CVPR)*, Jul. 2017, pp. 5967–5976.
[25] Y. Choi, M. Choi, M. Kim, J.-W. Ha, S. Kim, and J. Choo, "StarGAN: Unified generative adversarial networks for multi-domain image-to-image translation," in *Proc. IEEE/CVF Conf. Comput. Vis. Pattern Recognit.*, Jun. 2018, pp. 8789–8797.
[26] A. Creswell, T. White, V. Dumoulin, K. Arulkumaran, B. Sengupta, and A. A. Bharath, "Generative adversarial networks: An overview," *IEEE Signal Process. Mag.*, vol. 35, no. 1, pp. 53–56, Jan. 2018.
[27] D. Kinga and B. Adam, "Adam: A method for stochastic optimization," in *Proc. Int. Conf. Learn. Represent. (ICLR)*, vol. 5, 2015, pp. 1–15.
[28] L. Van der Maaten and G. Hinton, "Visualizing data using t-SNE," *J. Mach. Learn. Res.*, vol. 1, pp. 1–48, Nov. 2008.

XIAOJIE FAN received the bachelor's degree in communication engineering from the University of Science and Technology Beijing, Beijing, China, in 2017, where he is currently pursuing the Ph.D. degree with the School of Computer and Communication Engineering. His research interests include optical communication and deep learning.

FANG REN received the bachelor's and master's degrees in electronic science and technology from Tianjin University, Tianjin, China, in 2008 and 2010, respectively, and the Ph.D. degree in information electronics from Hokkaido University, Sapporo, Japan, in 2014. Her research interests include optical communication systems, optical devices, and deep learning.

JINGYU ZHANG received the bachelor's degree in communication engineering from the University of Science and Technology Beijing, Beijing, China, in 2019, where she is currently pursuing the master's degree with the School of Computer and Communication Engineering. Her research interests include deep learning and robotics.

YIYING ZHANG received the bachelor's degree in communication engineering from the University of Science and Technology Beijing, Beijing, China, in 2015, where she is currently pursuing the Ph.D. degree with the School of Computer and Communication Engineering. Her research interest includes optical communications.

JINGJING NIU received the bachelor's degree in communication engineering from the University of Science and Technology Beijing, Beijing, China, in 2019, where she is currently pursuing the master's degree with the School of Computer and Communication Engineering. Her research interest includes optical communications.

JIANPING WANG received the bachelor's, master's, and Ph.D. degrees from the School of Precision Instrument and Optoelectronic Engineering, Tianjin University, Tianjin, China, in 1995, 1997, and 2000, respectively. Her research interests include optical communications, microwave photonics, and deep learning.